Absolute cross sections for the photoionization of atomic oxygen: 2*s*-electron ionization and satellite production in the threshold energy range

O. Wilhelmi, G. Mentzel, B. Zimmermann, and K.-H. Schartner
I. Physikalisches Institut, Justus-Liebig-Universität, D-35392 Giessen, Germany

H. Liebel and H. Schmoranzer
Fachbereich Physik, Universität Kaiserslautern, D-67663 Kaiserslautern, Germany

B. M. McLaughlin
Department of Applied Mathematics and Theoretical Physics, The Queen's University of Belfast, Belfast BT7 1NN, Northern Ireland
(Received 5 May 1999)

Absolute cross sections for $2s$-electron photoionization of atomic oxygen into the final ionic states O^+ ($2s^{-1}\,{}^4P^e$, ${}^2D^e$, ${}^2S^e$, ${}^2P^e$) and for the occupation of the O^+ ($3s\,{}^{2,4}P^e$) satellite states have been determined experimentally by photon-induced fluorescence spectroscopy. Comparison of the experimental results with theoretical predictions using multiconfiguration-interaction wavefunctions employing the *ab initio R*-matrix technique are made. Suitable harmony is seen only in the case of cross section ratios for $2s^{-1}$ removal or $3s$-satellite excitation. [S1050-2947(99)02011-9]

PACS number(s): 32.80.Fb, 32.80.Dz

I. INTRODUCTION

Photoionization cross-section data of atomic oxygen is of vital importance for many applications in astrophysical, ionospheric, and atmospheric physics. Atomic oxygen is seen to play a key role in the chemistry cycle of the terrestrial ionosphere [1]. Extreme ultraviolet radiation from the sun ionizes thermospheric constituents, resulting in the formation and heating of the ionosphere over much of the planet. The primary source of energetic electrons and ions in the daytime thermosphere is from the photoionization of atomic oxygen. Photoelectrons from atomic oxygen provide the major source of heating in the daytime mid-latitude ionosphere. Additionally, photoionization of atomic oxygen is of great importance in the formation of the F layers in the Earth's ionosphere. In this region electrons can travel for long distances, spiraling along the lines of force of the earths magnetic field [2].

The total rate of electron production depends on the total cross section, but individual cross sections are required to calculate the energy distribution of the photoelectrons and the intensities of the spectral lines which can be emitted following the production of the atomic oxygen ion O^+ in excited states. Remote sensing of the atmosphere using selected emissions in the far-ultraviolet band continues to be an area of intense effort, motivated by the goal of continuous monitoring of ionospheric densities and temperatures from space [3–5]. The F region of the earth's ionosphere can be sensed remotely by measuring features produced by radiative recombination of atomic oxygen ions, the inverse process of photoionization. The densities and temperatures of atmospheric and ionospheric species can be deduced by measuring emissions of known origin and photochemistry traceable to the species in question and by using inversion techniques [4, 6].

It is well established that cross sections for individual transitions are used in predicting electron temperature in the ionosphere [7] and in predicting the intensities of ionic emission lines arising from fluorescence [8]. As pointed out by Bell and co-workers, considerable effort, both theoretical and experimental has been dedicated towards obtaining total cross sections [9–11] for photoionization of neutral atomic oxygen. However, there is still a lack of available experimental data for the individual transitions which leaves the final O^+ ion in the $2s2p^4\ {}^4P^e$, ${}^2D^e$, ${}^2S^e$, and ${}^2P^e$ states or the $3s\ {}^4P^e$ and $3s\ {}^2P^e$ states.

In the present study photon-induced fluorescence spectroscopy (PIFS) was applied to measure absolute cross sections for the photoionization out of the $2s^2 2p^4\ {}^3P^e$ ground state of atomic oxygen. For the various individual transitions investigated experimentally, comparisons are made with theoretical predictions on atomic oxygen. The theoretical calculations are performed using the *ab initio R*-matrix method employing multiconfiguration target wave functions for the initial and final states of the collision complex. Cross sections were determined for the photoionization of a $2s$ electron into the final ionic states,

$$O({}^3P^e) + h\nu_{SR} \rightarrow O^+(2s\,2p^4\ {}^4P^e, {}^2D^e, {}^2S^e, {}^2P^e) + e^-, \tag{1}$$

and for the population of the $3s\ {}^{2,4}P^e$ satellite states of O^+, namely,

$$O({}^3P^e) + h\nu_{SR} \rightarrow O^+(2s^2\,2p^2({}^3P)3s\ {}^4P^e, {}^2P^e) + e^-, \tag{2}$$

where ν_{SR} is the frequency of the synchrotron radiation photons. The final ionic states relax via radiative transitions. The fluorescence emitted in these transitions was detected in the present experimental arrangement. The various decay processes of the photoionized atomic oxygen ion may be summarized as follows:

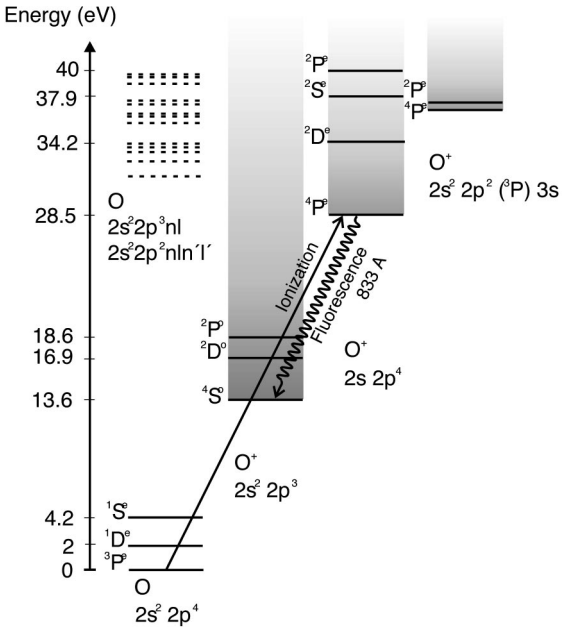

FIG. 1. Energy-level scheme for states of neutral and singly ionized atomic oxygen including the ionic state continua. Energy levels are taken from Striganov and Sventitskii [12], and assigned by electron configurations. For neutral atomic oxygen a few excited states are included as examples. One example of photoionization followed by radiative fluorescence decay is illustrated.

$$O^+(2s2p^4\ ^4P^e,^2D^e,^2S^e,^2P^e)$$

$$\downarrow$$

$$O^+(2s^22p^3\ ^4S^o,^2D^o,^2P^o)+h\nu_{\rm fl}$$

and

$$O^+(2s^22p^2(^3P)3s\ ^4P^e,^2P^e)$$

$$\downarrow$$

$$O^+(2s^22p^3\ ^4S^o,^2D^o,^2P^o)+h\nu_{\rm fl}, \qquad (3)$$

where $\nu_{\rm fl}$ is the frequency of the fluorescence photons.

Figure 1 shows an energy-level scheme with one example illustrating a $2s$-electron ionization followed by fluorescent decay of the final O^+ state. All of the atomic processes investigated here in detail are listed in Table I, where we also include the energy of the exciting synchrotron radiation and the fluorescent transition wavelength of the subsequent O^+ states produced in the photoionization processes.

Since there are no competitive, nonradiative relaxation processes and the exciting photon energies do not allow cascade population from energetically higher ionic states, the fluorescence intensities of the radiative transitions are proportional therefore to the partial photoionization cross sections. For photoionization into the $O^+(2s2p^4\ ^4P^e)$ state of singly ionized atomic oxygen, a cross section for the dissociative ionization process from molecular oxygen was also possible to be determined, namely, for the process

$$O_2(X\ ^3\Sigma_g^-)+h\nu_{\rm SR}\rightarrow O+O^+(2s2p^4\ ^4P^e)+e^-. \qquad (4)$$

TABLE I. Photoionization processes in atomic oxygen investigated in the present study. The synchrotron radiation energy $h\nu_{\rm SR}$ necessary to reach the excited singly ionized state is given in eV, and the fluorescence wavelength λ (in units of Å) for the transition into the final ionic state [12] are included for completeness.

Ground state	Excited ionic state Threshold energy (eV)	Final ionic state Fluorescence wavelength (Å)
$O(2s^22p^4\ ^3P^e)$	$O^+(2s2p^4\ ^4P^e)$	$O^+(2s^22p^3\ ^4S^o)$
	$h\nu_{\rm SR}\geqslant 28.5$ eV	λ = 833 Å
	$O^+(2s2p^4\ ^2D^e)$	$O^+(2s^22p^3\ ^2D^o,^2P^o)$
	$h\nu_{\rm SR}\geqslant 34.2$ eV	λ = 719 Å,797 Å
	$O^+(2s2p^4\ ^2S^e)$	$O^+(2s^22p^3\ ^2P^o)$
	$h\nu_{\rm SR}\geqslant 37.9$ eV	λ = 644 Å
	$O^+(2s2p^4\ ^2P^e)$	$O^+(2s^22p^3\ ^2D^o,^2P^o)$
	$h\nu_{\rm SR}\geqslant 40.0$ eV	λ = 538 Å,581 Å
	$O^+(2s^22p^2(^3P)3s\ ^4P^e)$	$O^+(2s^22p^3\ ^4S^o)$
	$h\nu_{\rm SR}\geqslant 36.6$ eV	λ = 539 Å
	$O^+(2s^22p^2(^3P)3s\ ^2P^e)$	$O^+(2s^22p^3\ ^2D^o,^2P^o)$
	$h\nu_{\rm SR}\geqslant 37.1$ eV	λ = 617 Å,673 Å

II. EXPERIMENT

A. Overview

To obtain absolute experimental cross sections for the photoionization of atomic oxygen by PIFS, an atomic oxygen source was set up at the synchrotron radiation facility BESSY I. Atomic oxygen was provided by a microwave-driven discharge source. Atomic and molecular oxygen emerging from that source in an effusive beam was intersected by a beam of synchrotron radiation. A schematic diagram of the atomic oxygen source is illustrated in Fig. 2.

Fluorescence emitted in transitions of excited ionic states was dispersed in the vacuum ultraviolet (VUV) spectral re-

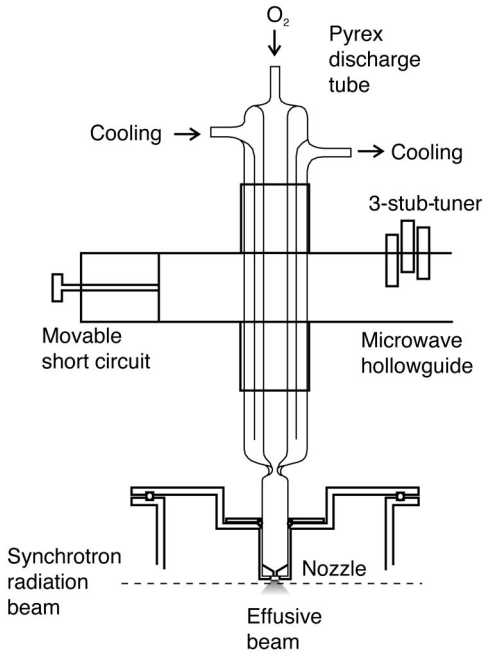

FIG. 2. Atomic oxygen source used in the present experiment.

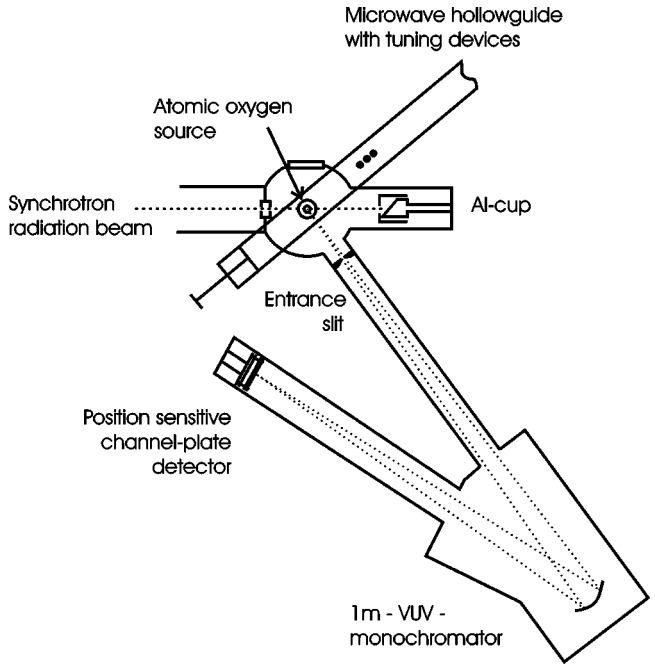

FIG. 3. Top view of the experimental setup.

gion by a 1-m normal-incidence monochromator. A two-dimensional position sensitive detector mounted in the position of the exit slit was allowed to simultaneously register fluorescence from different transitions (Fig. 3). Fluorescence intensities were recorded in dependence of the synchrotron radiation energy. Normalization to absolute cross sections was carried out by comparison to a photoionization cross section in argon.

B. Atomic oxygen source — setup

The atomic oxygen source consists of a pyrex discharge tube stuck through a microwave hollow guide (Fig. 2). A 2.45-GHz microwave with 120 W power travels through a rectangular hollow guide terminated by a movable short circuit. Incident and reflected waves interfere to yield a standing-wave pattern. By moving the short circuit, an electric-field maximum can be put to the discharge tube. Impedance matching is achieved by a three-stub tuner.

A constant mass flow of 1 sccm molecular oxygen is fed to the pyrex discharge tube by a mass flow controller. The discharge tube is 18 mm in diameter, and can be cooled by a flow of cold nitrogen vapor, produced by electric heating of liquid nitrogen in a closed dewar container. The extension of the discharge is limited by a 6-mm aperture separating the discharge from a 95-mm-long exit channel. At the end of the exit channel is a teflon nozzle, with dimensions 0.8 mm in diameter and 3 mm long, forming the effusive beam and maintaining the pressure difference between discharge tube and interaction region, where the source pressure is estimated to be approximately 0.8 mbar. In order to improve the degree of dissociation in the molecular oxygen discharge, a small amount (5–7%) of methane (CH_4) was added to the mass flow.

C. Atomic oxygen source — operation parameters

In the molecular oxygen discharge only a certain percentage of the O_2 molecules are dissociated, so the effusive beam consists of atoms and molecules. In order to separate the fluorescence signal originating from photoionization of atoms and molecules of oxygen into the same final ionic states, the composition of the effusive beam has to be known.

The most important parameter is the degree of dissociation D, i.e., the ratio of dissociated molecules to the molecules fed to the discharge. The degree of dissociation cannot be extracted from the fluorescence data in the photoionization experiment described here. It was determined by intersecting the effusive beam with a 3-keV electron beam, keeping all the discharge parameters constant. Fluorescence from excited oxygen atoms for the transition $O(2s^2 2p^3(^2P^o)3s\ ^1P^o) \rightarrow O(2s^2 2p^4\ ^1D^e)$ at 999 Å was detected, having the discharge turned on and off. Since excitation by 3-keV electrons obeys optical dipole selection rules, singlet states cannot be excited from atomic oxygen triplet ground state O ($^3P^e$). Therefore, fluorescence from that singlet transition results from dissociative excitation of molecules. When turning the discharge on, a decrease in this fluorescence intensity is observed, which indicates a decrease of O_2 molecules in the effusive beam due to dissociation. The relative decrease of intensity from dissociative excitation gives the relative decrease of O_2 molecules in the effusive beam. The degree of dissociation D is therefore derived from the intensity ratio of the line at 999 Å with the discharge on and off:

$$D = 1 - \frac{I^{999\ \text{Å}}_{\text{discharge on}}}{I^{999\ \text{Å}}_{\text{discharge off}}}. \tag{5}$$

The electron impact experiment gives a degree of dissociation of about

$$D \approx 0.30,$$

i.e., a mass flow of 1 sccm O_2 molecules fed to the discharge, splits up into a mass flow of $2 \times 0.3\ \text{sccm} = 0.6\ \text{sccm}$ atoms and 0.7 sccm molecules. The density of oxygen atoms in the interaction region, taken from an effusive beam simulation [13] is in the order of magnitude of $2 \times 10^{13}\ \text{cm}^{-3}$.

The results of this experiment do not give any evidence of atomic oxygen in metastable O ($^1D^e$) or O ($^1S^e$) states in the effusive beam (cf. Sec. V C). A small amount of molecular oxygen in the metastable O_2 ($a\ ^1\Delta_g$) state, found in our electron-impact measurements [14] is assumed to be negligible. In the electron-impact measurement fluorescence from the first and second negative band system of O_2^+ was observed in the visible and near-ultraviolet spectral range (670–265 nm) simultaneously to the VUV fluorescence, to verify the degree of dissociation and the absence of metastable molecular states. To check for ionized atomic oxygen in the effusive beam, fluorescence from doubly ionized atomic oxygen was investigated in the electron-impact measurements. The weak fluorescence intensity observed from radiative transitions in doubly ionized atomic oxygen is attributed to double ionization of atomic oxygen, because of a cross-section estimation based on the total cross-section ratio for single and double ionization of atomic oxygen [15]. We conclude that atomic oxygen ions are neutralized in the nozzle.

The analysis of the constituents of the effusive beam is in agreement with similar experiments [16–22], and justifies the assumption that the effusive beam consists only of electronic ground state oxygen atoms and molecules, namely, $O(^3P^e)$ and O_2 $(X\ ^3\Sigma_g^-)$.

D. Synchrotron radiation beamline

Experiments were carried out at the U2-FSGM-undulator beamline at BESSY I. Using both of the two crossed undulators, the beamline provided sufficient photon flux for a PIFS experiment on atomic oxygen. Due to the weak fluorescence intensity, the exit slit of the FSGM monochromator had to be set to 1500 μm, resulting in an exciting photon energy bandwidth of about 100 meV full width at half maximum (FWHM) at energies between 28 and 42 eV. A step width of 100 meV in the exciting photon energy was chosen in our experiment. The photon flux transmitted through the experimental setup was monitored by the electric current of an Al-photon cup, and amounts to 10^{11} photons per second. The photon flux in higher-order synchrotron radiation is neglected (due to the weak fluorescence intensity at exciting photon energies below threshold in Figs. 5, 6, and 7) and the energy scale of the exciting photons is fixed by the energies of the ionization thresholds.

E. Fluorescence detection

The synchrotron radiation beam intersected the effusive beam from the atomic oxygen source 3 mm below the nozzle exit. The intersection position was fixed by five aligned circular apertures (the smallest one 2.5 mm in diameter). The fluorescence from the transitions in O^+ produced after photoionization or dissociative ionization, was dispersed by a 1-m normal-incidence monochromator, mounted under the magic angle with respect to the synchrotron radiation beam (Fig. 3). The magic angle mount suppressed the influence of the angular distribution of the fluorescence. The monochromator was equipped with a 1200 lines per mm osmium coated grating, blazed at 600 Å. The observed fluorescence wavelength ranged from 400 to 1250 Å. The use of a two-dimensional position sensitive multichannel-plate detector allowed the detection of a spectral range of around 350 Å simultaneously. The entrance slit of the 1-m normal-incidence monochromator was set to 400 μm, giving a resolving power of about 200.

The photoionization experiments were performed on an effusive beam with discharge on and on a pure molecular oxygen beam with discharge off [Figs. 4(a) and 4(b)]. The fluorescence intensity from the molecules in the effusive beam was subtracted, using the degree of dissociation D, to obtain the fluorescence intensities originating from photoionization of atomic oxygen only [Fig. 4(c)]. The resulting intensity was normalized to the atomic mass flow.

$$I_{\text{atom}}=\frac{I_{\text{discharge on}}-(1-D)I_{\text{discharge off}}}{2DM}, \tag{6}$$

where M is the mass flow.

From Figs. 4(a), 4(b), and 4(c), it becomes evident, that this subtraction could only be performed for the fluorescence intensity at the wavelength of 833 Å. Since dissociative $2s$-electron ionization from the molecular oxygen O_2 $(X\ ^3\Sigma_g^-)$ ground state needs exciting photon energies of at least 5.1 eV dissociation energy above the atomic $2s$-electron ionization thresholds (cf. Fig. 1), dissociative ionization can only occur for the O^+ $(2s2p^4\ ^4P^e,^2D^e)$ states over the photon energy range considered here. Due to its very weak fluorescence intensity, dissociative ionization into the O^+ $(2s2p^4\ ^2D^e)$ state was supposed to be negligible.

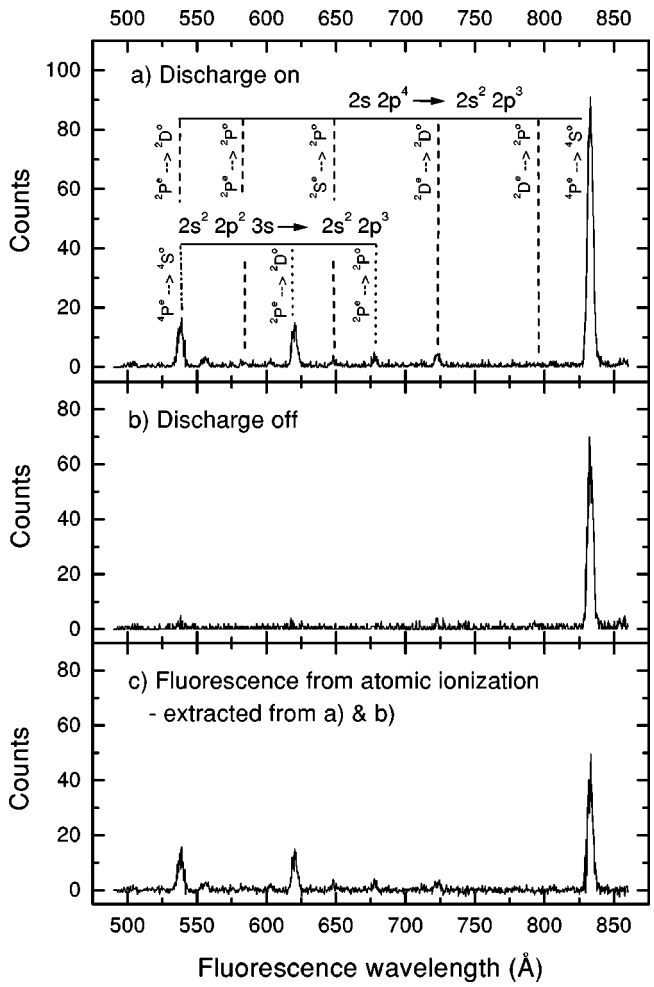

FIG. 4. VUV spectra in the wavelength range 490–860 Å at the exciting photon energy of 41.44 eV. The counts collected in about 25 min are displayed. (a) The spectrum recorded from an effusive beam from the burning discharge. (b) The spectrum recorded from a pure molecular oxygen effusive beam. (c) The fluorescence resulting from the atoms in the effusive beam from the burning discharge and extracted from the spectra of (a) and (b). The very low fluorescence intensity can be seen from the accumulated counts (not normalized to atomic mass flow).

The fluorescence intensity for each transition was corrected for the relative quantum efficiency of the grating-detector system and normalized to the exciting photon flux. The exciting photon energy was scanned in 100-meV steps. This scanning was repeated three times in two different measuring periods at BESSY I. The integration time per step was a few minutes in each scan. Additionally, spectra were recorded at selected energies with an integration time of 30 min to obtain information about transitions of very weak fluorescence intensities and to yield better statistics.

F. Normalization procedure

The fluorescence intensities from photoionization of atomic oxygen were compared to the fluorescence intensity from the Ar $3s$-electron photoionization at 920 and 932 Å, measured under the same experimental conditions at the exciting photon energy of 30.5 eV. Setting the mass flow of Ar to that of O_2, the target density had to be corrected. The difference in target density results from the difference in particle velocity due to the masses of O, O_2, and Ar. A simulation of the effusive beams for O, O_2, and Ar [13] showed no significant differences in the effusive beam profiles. The three different scans have been averaged and then normalized to the absolute cross section of Ar $3s$-electron photoionization 0.79 Mb [23].

III. THEORETICAL OVERVIEW

The success of *ab initio R*-matrix methods in the study of valence shell photoionization from the O ($^3P^e$) ground state and the O ($^1D^e$) and O ($^1S^e$) excited states of atomic oxygen is well documented in the literature [24,11,10,9,25], where it is seen that there is a degree of harmony between the available theoretical and experimental work [16,26]. Further details may be found in the review article of Bell and Kingston [11]. For the valence shell processes the range of photon energies extends to 275.5 eV (45 Å) in previous *ab initio* studies [11,10] and to 212 eV (58.5 Å) in experimental studies [16]. In the case of the Auger processes, in particular for $1s^{-1}$ removal, the relevant photon energy range extends from 525 to 560 eV as noted in recent experimental work [27,16,28,18]. *Ab initio* studies have been made recently [29] using the *R*-matrix approach to investigate and provide information on cross sections for the *K*-shell excitation and ionization from the ground state of atomic oxygen $O(1s^2 2s^2 2p^4\ ^3P^e)$, where the processes

$$h\nu + O(^3P^e) \rightarrow O^*(1s2s^2 2p^4(^{2,4}P^e)np\ ^3P^o)$$
$$\searrow \qquad \downarrow$$
$$O^+(1s2s^2 2p^4(^{2,4}P^e)) + e^-$$

were studied in detail. Cross-section calculations for the photoabsorption process were carried out in both the length and velocity gauges with agreement achieved to within a few percent. In the vicinity of the oxygen *K* edge, a suitable accord with the available synchrotron experimental data [28,18], was achieved. The theoretical calculations of McLaughlin and Kirby [29] treated not only the $1s^{-1}$ removal processes, but also include the valence shell processes involving $2s^{-1}$ and $2p^{-1}$ removal and production of the O^+ ($3s\ ^{2,4}P^e$) satellite states which are presented here.

The theoretical predictions of McLaughlin and Kirby [29] extend the work of Bell and co-workers to the region of the *K* edge and are of similar quality in the valence region, as can be seen from Table II, where comparisons are made for the available cross-section ratios for $2p^{-1}$ removal. Theoretical partial cross sections for $2s^{-1}$ removal or population of the O^+ ($3s\ ^{2,4}P^e$) satellite states, based on the work of McLaughlin and Kirby [29] (that includes 15 final states of the O^+ ion) are presented and compared with the current experimental observations made at BESSY I.

TABLE II. Comparison of various theoretical and experimental branching ratios.

Wavelength λ (Å)	Reference	$\sigma(2p^{-1}\ ^2D^o)/\sigma(2p^{-1}\ ^4S^o)$	$\sigma(2p^{-1}\ ^2P^o)/\sigma(2p^{-1}\ ^4S^o)$
584	Present	1.47	0.69
	Ref. [10]	1.46	0.68
	Ref. [30]	1.29	0.81
	Ref. [31]	1.48 (1.19)[a]	0.95 (0.66)
	Ref. [32]	1.54 (1.59)	0.92 (0.86)
	Ref. [17]	1.57 ± 0.4	0.82 ± 0.07
304	Present	1.67	0.97
	Ref. [10]	1.71	0.99
	Ref. [30]	1.18	1.34
	Ref. [31]	1.49 (1.42)	0.99 (0.91)
	Ref. [32]	1.33 (1.62)	0.85 (0.89)
	Ref. [33]	1.65 ± 0.15	0.93 ± 0.10

[a]Values in parentheses are velocity formulation results.

IV. RESULTS

The experimental cross sections for the photoionization processes in Table I are presented with the results of the calculations in Figs. 5, 6, and 7. Convolutions of the calculated cross sections with a Gaussian function of 100-meV FWHM of the exciting photons are also displayed to allow a comparison with the experimental data. The fluorescence occurring in the case of the final O^+ ($2s^{-1}\ ^2P^e$) and O^+ ($2s^{-1}\ ^2S^e$) ionic states was extremely weak; it was only analyzed in the resulting spectra at certain exciting photon energies.

According to Table I, there are two radiative decay channels of O^+ ($2s^{-1}\ ^2P^e$) with fluorescence wavelengths of 581 and 538 Å. The fluorescence at 538 Å was not resolved from the fluorescence of the O^+ ($3s\ ^4P^e$) satellite state at 539 Å. To obtain the cross section for photoionization into O^+ ($2s^{-1}\ ^2P^e$), the branching ratio for the two radiative decay channels $I(538\ \text{Å})/I(581\ \text{Å}) = 4.0$ [34] was applied to get the fluorescence intensity at 538 Å. From the weak intensity of the fluorescence line at 581 Å it can be concluded, that most of the intensity at 538 Å/539 Å results from the decay of the satellite $3s\ ^4P^e$ state [Fig. 4(c)]. Furthermore, in Fig. 7 the threshold for the O^+ ($3s\ ^4P^e$) satellite excitation at 36.6 eV can clearly be seen in the experiment, whereas here is no hint of the O^+ ($2s^{-1}\ ^2P^e$) photoionization threshold at 40.0 eV.

A. Experimental uncertainties

The error bars of the experimental data represent the statistical error of Eq. (6): the double standard deviations of the fluorescence intensity signals $I_{\text{discharge on}}$ and $I_{\text{discharge off}}$, and the statistical variations of mass flow and degree of dissociation *D* are summed. The statistical error from intensity normalization to the exciting photon flux is included. The subtraction of the $I_{\text{discharge off}}$ signal had only to be carried out for the O^+ ($2s^{-1}\ ^4P^e$) cross section.

The relative systematic error of the normalization procedure was determined by the relative error of the Ar $3s$-electron photoionization cross section, the relative statistical error of the normalization measurement, the relative er-

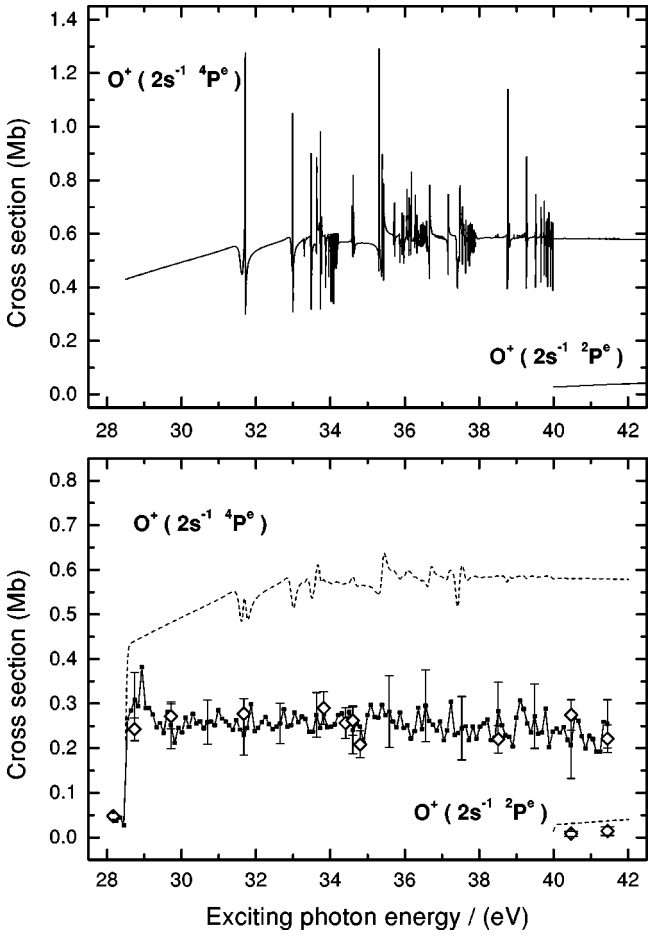

FIG. 5. Experimental and theoretical cross sections for O^+ $(2s^{-1}\,{}^4P^e)$ and O^+ $(2s^{-1}\,{}^2P^e)$ photoionization. The solid lines are the *ab initio R*-matrix calculations (top graph), and the dashed lines (bottom graph) represent the convolution with a Gaussian function of 100-meV experimental energy resolution half-width. The solid squares are taken from the 100-meV scanning experiment, and the open diamonds are taken from the measured spectra. Error bars include statistical errors only.

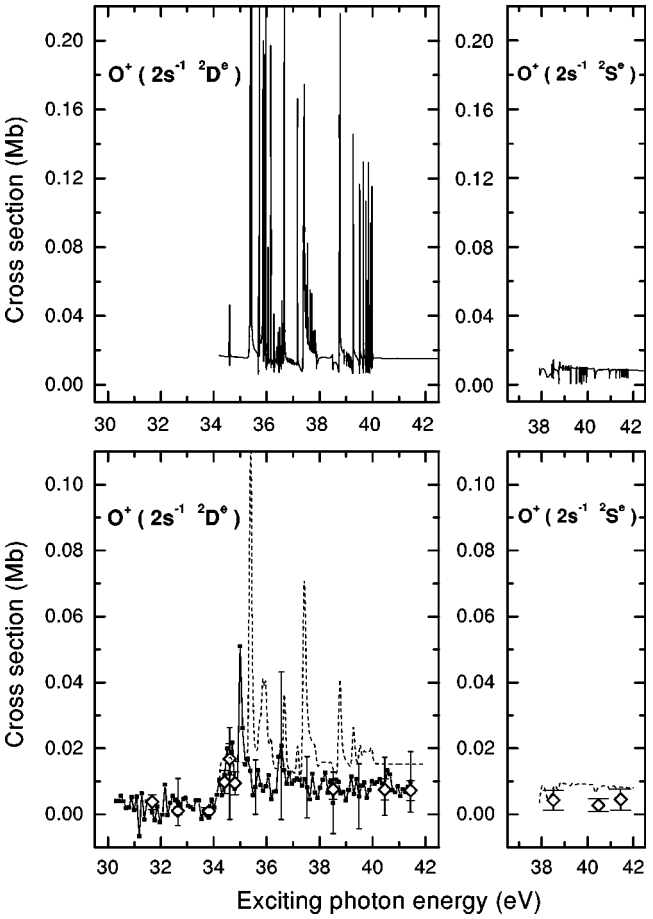

FIG. 6. Experimental and theoretical cross sections for O^+ $(2s^{-1}\,{}^2D^e)$ and O^+ $(2s^{-1}\,{}^2S^e)$ photoionization. The solid lines are the *ab initio R*-matrix calculations (top graphs), and the dashed lines (bottom graphs) represent the convolution with a Gaussian function of 100-meV experimental energy resolution half-width. The solid squares are taken from the 100-meV scanning experiment, and the open diamonds are taken from the measured spectra. Error bars include statistical errors only.

ror of the degree of dissociation, and the relative error of the quantum efficiency correction for the different fluorescence wavelengths. The latter error could even affect the cross-section ratios. The contributions to the total systematic error are listed in Table III.

Variations in the intersection of effusive beam and synchrotron radiation beam within the area fixed by the apertures (cf. Sec. II E) have to be taken into consideration. Although no significant changes in this intersection have been observed while scanning the exciting photon energy, even after successive electron injections at BESSY I, a systematic error for normalization to the Ar $3s$-electron photoionization cross section was determined, simulating different overlaps of synchrotron radiation beam and effusive beams for Ar and O/O_2. The maximum deviation amounts to a relative systematic error of 27%. It has to be noted here that the effusive beam simulation [13] used to check the density distribution could not be applied to an effusive beam containing atomic and molecular oxygen at once. Nevertheless, experimental tests have proved reliability of combining separate simulations for effusive beams with atoms and molecules. Regarding all the systematic errors listed in Table III, the present experimental arrangement cannot deliver absolute photoionization cross sections more accurate than within a factor 2.

V. DISCUSSION

A. Experimental and theoretical off-resonance cross sections

The theoretical cross sections for $2s$-electron photoionization are larger than the experimental cross sections. They are seen to differ by a factor 2 (Figs. 5 and 6). Given the fact that the absolute values of the cross sections of the present calculations are in good agreement with the earlier work of Bell and co-workers, it would indicate that this deviation is due to a systematic error in the normalization of the measured fluorescence intensities to absolute cross sections. However, the experimental cross-section ratios do agree well with the theoretical predictions. On the other hand, we note that the magnitude of the theoretical cross sections for production of the O^+ $(3s\,{}^{2,4}P^e)$ satellite excitations are smaller than the experimental values (Fig. 7).

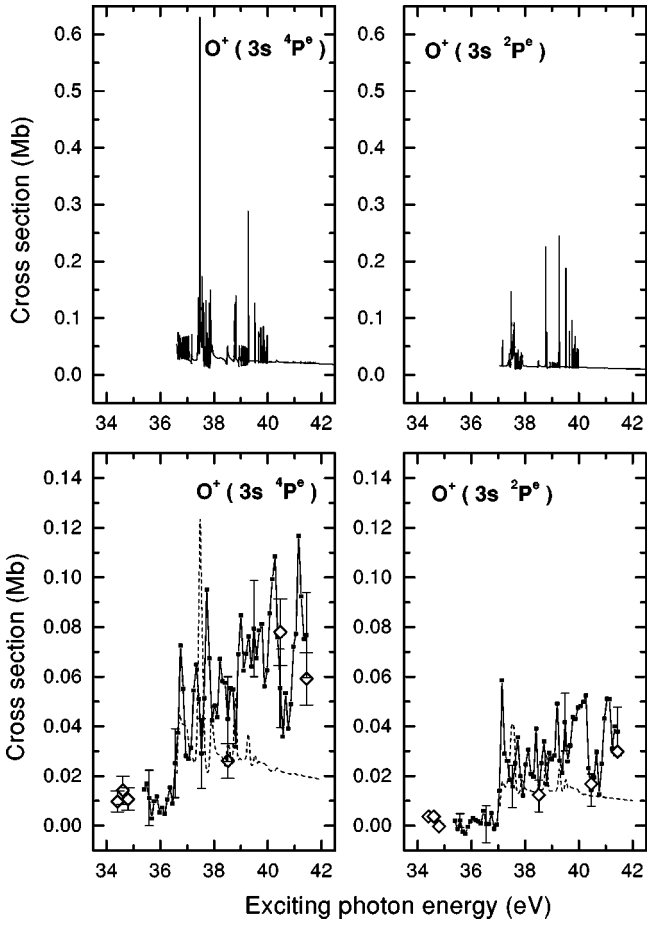

FIG. 7. Experimental and theoretical photoionization cross sections for the excitation of the O^+ $(3s\ ^{2,4}P^e)$ satellite states. The solid lines are the *ab initio R*-matrix calculations (top graphs), and the dashed lines (bottom graphs) represent the convolution with a Gaussian function of 100-meV experimental energy resolution half-width. The solid squares are taken from the 100-meV scanning experiment, and the open diamonds are taken from the measured spectra. Error bars include statistical errors only.

B. Autoionization resonances

Atomic oxygen is an open-shell atom; therefore, resonance structure may result from two types of autoionizing excited states caused by the incident photon having sufficient energy to excite one or more electrons to Rydberg states. One electron excitations manifest themselves in the theoretical predictions as Rydberg series O $(2s2p^4(^2D^e)np\ ^3P^o,^3D^o)$, O $(2s2p^4(^2S^e)np\ ^3S^o,^3P^o)$, and O $(2s2p^4(^2P^e)np\ ^3S^o,^3P^o,^3D^o)$, converging to their respective ionic core thresholds. Resonances due to autoionization of doubly excited states, like in the case of the $2s$-electron photoionization of neon [35], show up in the theoretical cross sections as Rydberg series converging to satellite thresholds, e.g., O $(2s^22p^2(^3P)3s(^4P^e,^2P^e)ns/nd\ ^3S^o,^3P^o,^3D^o)$. The variety of coupling possibilities gives rise to resonance structure more complicated than in the case of the rare gases.

TABLE III. Contributions to the total systematic error.

Source of systematic error	Amount
Reference cross section [23]	19%
Degree of dissociation	16%
Normalization measurement	6%
Quantum efficiency correction	23%
Variation of beam intersection	27%
Sum	91%

The convolution of the dominant O^+ $(2s^{-1}\ ^4P^e)$ cross section with the exciting photon bandwidth shows that the rich resonance structure, due to autoionizing excited states of atomic oxygen which is evident in the theoretical predictions, cannot be stringently tested by the present experiment where the energy resolution of the exciting photon is limited to 100 meV (Fig. 5). The few clear resonance features remaining in the convolution of the theoretical cross section do not reproduce the hints of autoionization resonances in the experimental cross section. For photoionization into the O^+ $(2s^{-1}\ ^4P^e)$ ionic state, experiment shows an enhancement close to threshold. Conversely, theory does not show any resonance structure at such exciting photon energies, but increases linearly from threshold to the first resonance.

The experimental photoionization cross section for production of the O^+ $(2s^{-1}\ ^2D^e)$ ionic state (Fig. 6), shows a pronounced resonance structure close to threshold, as does excitation of the O^+ $(3s\ ^{2,4}P^e)$ satellite states (Fig. 7). A test of the detailed resonance structure found in the theoretical predictions requires a much higher resolution measurement, which could not be performed at the target density and exciting photon flux achieved with the present experimental setup.

C. O^+ $(2s^{-1}\ ^2D^e)$ and O^+ $(2s^{-1}\ ^2S^e)$ cross sections

Figure 6 shows the cross sections for $2s$-electron photoionization from the O $(^3P^e)$ ground state into the O^+ $(2s^{-1}\ ^2D^e)$ and O^+ $(2s^{-1}\ ^2S^e)$ ionic states. Assuming LS coupling in the picture of the independent-electron model, both transitions are not allowed since the $2s$ electron ejected has no angular momentum before the photoionization. Therefore its photoionization should not affect the total angular momentum, i.e., $2s^{-1}$ ionization from the O $(^3P^e)$ ground state should lead to O^+ $(2s^{-1}\ ^4P^e)$ and O^+ $(2s^{-1}\ ^2P^e)$ ionic states only. In earlier investigations of the $2s$-electron photoionization, only these ionization channels have been discussed [16,36].

To examine the photoionization from O $(^3P^e)$ to the O^+ $(2s^{-1}\ ^2D^e)$ ionic state, the 719 Å fluorescence from the transition O^+ $(2s2p^4\ ^2D^e \rightarrow 2s^22p^3\ ^2D^o)$ was scanned in spite of its low intensity. The threshold at 34.2 eV indicates that the O^+ $(2s^{-1}\ ^2D^e)$ ionic state is indeed ionized from the O $(^3P^e)$ atomic oxygen ground state (cf. Fig. 1). Photoionization from the metastable atomic O $(^1D^e)$ state to O^+ $(2s^{-1}\ ^2D^e)$ would result in a threshold at 32 eV. Since no threshold is observed at 32 eV, while the cross section for the $2s^{-1}$ photoionization of the metastable state O $(^1D^e)$ of atomic oxygen is of the same order of magnitude as the corresponding cross section of the ground state O $(^3P^e)$ (concluded from calculations of the total photoionization cross section by Bell and co-workers [11,9]), we assume that the contribution of metastable atoms to the effusive beam can be neglected.

TABLE IV. Comparison of the ratios of experimental fluorescence intensities from the spectra in Fig. 4(c) with calculated transition probabilities for the respective excited ionic states.

Excited ionic state	Intensity ratio (experiment)	Transition probability ratio (theory)[a]
$O^+(2s2p^4\ ^2P^e)$	$I_{581\ Å}/I_{538\ Å}=0.25$ [34]	$\Sigma A_{581\ Å}/\Sigma A_{538\ Å}=0.30$
$O^+(2s2p^4\ ^2D^e)$	$I_{797\ Å}/I_{719\ Å}\approx 0$	$\Sigma A_{797\ Å}/\Sigma A_{719\ Å}=0.0094$
$O^+(2s^22p^2(^3P)3s\ ^2P^e)$	$I_{673\ Å}/I_{617\ Å}=0.19$	$\Sigma A_{673\ Å}/\Sigma A_{617\ Å}=0.16$

[a]Theoretical values from Ref. [37].

The O^+ $(2s^{-1}\ ^2D^e)$ and O^+ $(2s^{-1}\ ^2S^e)$ photoionization channels prove that the assumption of an independent-electron model in LS coupling does not hold. Theoretical predictions take this into account by using multiconfiguration interaction wave functions for both the ground state of the neutral atom and the final ionic states of atomic oxygen.

D. Fluorescence branching ratios

The fluorescence spectrum in Fig. 4(c), recorded at an exciting photon energy of 41.44 eV illustrates the intensities of the different radiative transitions listed in Table I. From the ionic states of atomic oxygen with two radiative decay channels, the branching ratios for the decay of O^+ $(2s2p^4\ ^2D^e)$ to O^+ $(2s^22p^3\ ^2D^o)$ at 719 Å and to O^+ $(2s^22p^3\ ^2P^o)$ at 797 Å, and the decay of O^+ $(2s^22p^2(^3P)3s\ ^2P^e)$ to O^+ $(2s^22p^3\ ^2D^o)$ at 617 Å and to O^+ $(2s^22p^3\ ^2P^o)$ at 673 Å have been determined from the spectrum. The branching ratio for the decay of O^+ $(2s2p^4\ ^2P^e)$ to O^+ $(2s^22p^3\ ^2P^o)$ at 581 Å and to O^+ $(2s^22p^3\ ^2D^o)$ at 538 Å cannot be extracted from experimental data, as the fluorescence line at 538 Å is not resolved from the more intensive fluorescence line at 539 Å resulting from the O^+ $(3s\ ^4P^e)$ satellite state. Comparing the present experimental branching ratios with the theoretical values [37], in Table IV, indicates agreement to better than 20%.

E. Cross-section ratios

In view of the unavoidably large systematic errors in the experimental measurements for the absolute cross sections, no helpful conclusions can be drawn, although a degree of harmony with experiment is clearly seen in the convoluted theoretical cross sections. Furthermore, the experimental resolution (100 meV) is clearly insufficient to resolve the autoionizing features predicted theoretically, which typically have energy widths less than 25 meV. However, information from cross section ratios is possible and has been shown to be constructive [16].

In Fig. 8, the ratio of the cross sections for ejection of a $2s$ electron in the photoionization process producing the O^+ $(2s^{-1}\ ^2P^e)$ and O^+ $(2s^{-1}\ ^4P^e)$ ionic states of atomic oxygen is compared with the previous work of Schaphorst *et al.* [16]. As pointed out above, the ratio of the O^+ $(2s^{-1}\ ^2P^e)$ to O^+ $(2s^{-1}\ ^4P^e)$ cross section derived from the experiment agrees with the results of the theoretical predictions presented here, although there is a difference in the absolute cross sections. Our ratio is smaller than the experimental and the theoretical multiconfiguration Hartree-Fock (MCHF) values given by Schaphorst *et al.* [16], but is in suitable agreement with values from an earlier R-matrix calculation [37]. The $\sigma(^2P^e)/\sigma(^4P^e)$ cross section ratio close to the O^+ $(2s^{-1}\ ^2P^e)$ photoionization threshold from present work as well as the result of Schaphorst *et al.* [16] is significantly smaller than the geometrical cross-section ratios derived from MCHF calculations, indicating that there is a deviation from the LS-coupling scheme (geometrical value) in this exciting photon energy range.

Furthermore, the sum of all the four $2s^{-1}$ photoionization cross sections can be compared to the sum of the $2p^{-1}$ cross sections [36]. The ratio of $2s^{-1}$ to $2p^{-1}$ photoionization cross sections is shown together with the earlier results of Schaphorst *et al.* [16] in Fig. 9. The difference between the present theoretical and experimental $2s$-electron photoionization cross sections can also be seen in the

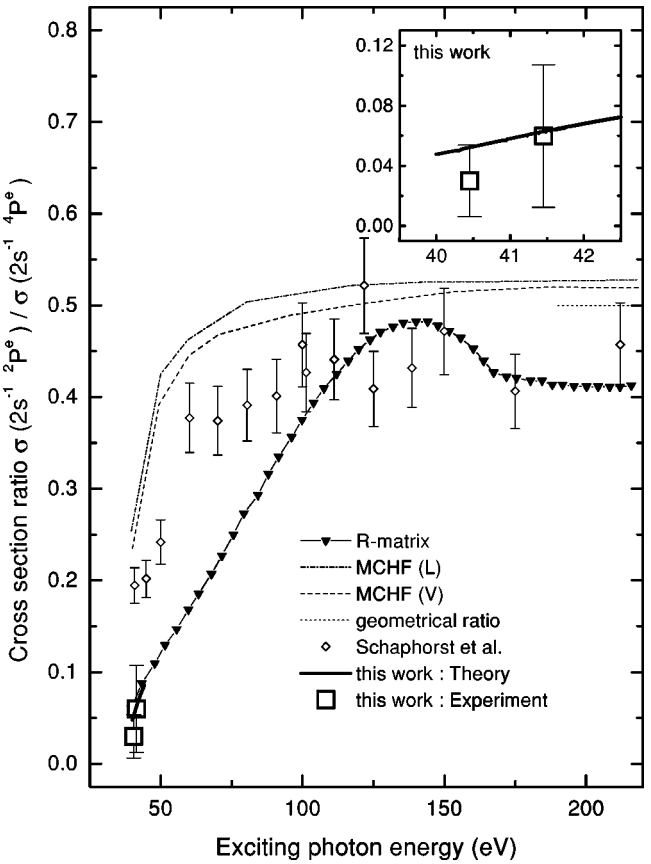

FIG. 8. Experimental and theoretical O^+ $(2s^{-1})$ $\sigma(^2P^e)/\sigma(^4P^e)$ photoionization cross-section ratio. Results are presented for an R-matrix [10] and multiconfiguration Hartree-Fock calculation [16] compared with the present experimental (only statistical error bars shown) and theoretical work and that of Schaphorst *et al.* [16] including the geometrical value.

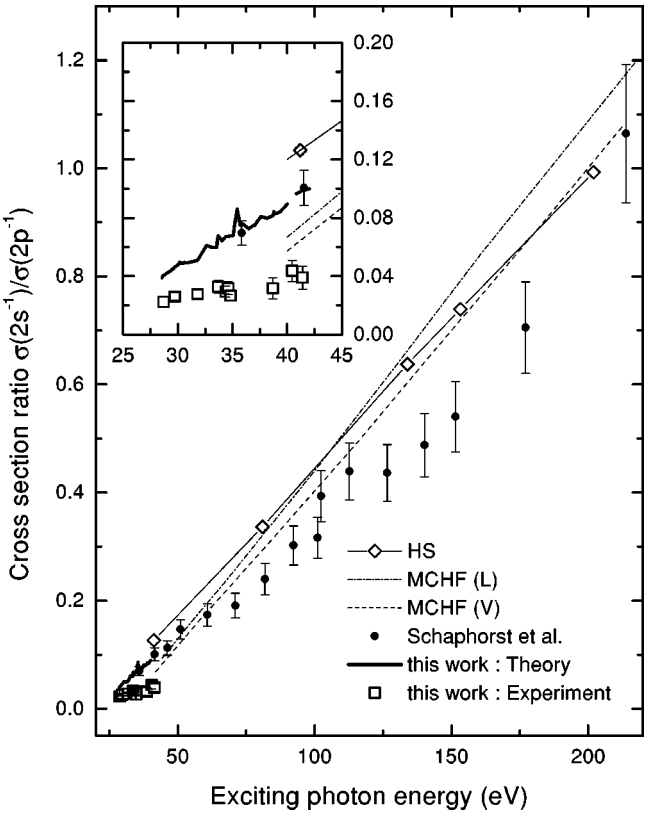

FIG. 9. Experimental and theoretical $O^+(2s^{-1})/O^+(2p^{-1})$ photoionization cross-section ratios. Results are presented for Hartree-Slater (HS) (from Ref. [16]) and multiconfiguration Hartree-Fock (MCHF) calculations [16] compared with the earlier findings of Schaphorst *et al.* [16] and the present theoretical and experimental work (only statistical error bars shown).

$\sigma(2s^{-1})/\sigma(2p^{-1})$ cross-section ratio. The cross-section ratio derived from our theoretical cross sections agrees well with the experimental data of Schaphorst *et al.* [16], supporting the theoretical cross sections and reinforcing the suggestion that our experimental data suffers a systematic error.

In contrast to the $2s^{-1}$ $\sigma(^2P^e)/\sigma(^4P^e)$ cross-section ratio, the theoretical cross section values for production of the satellite O^+ $(3s\,^2P^e, {}^4P^e)$ states in Fig. 7 at 42 eV, away from the resonant structure, yield a ratio of 0.5, which is the geometrical ratio. The experimental cross sections cannot be determined free from resonance influence, but their ratio seems to correspond to the geometrical ratio predicted by theory as well.

Although agreement of experimental and theoretical cross section ratios for $2s^{-1}$ removal on the one hand and for $3s$-satellite excitation on the other is observed, contradiction between experiment and theory has to be stated for the ratio of $2s^{-1}$ removal cross section to $3s$-satellite excitation cross section (Figs. 5, 6 and 7).

F. Dissociative ionization

In the scans taken with the discharge turned off, the fluorescence occurring at 833 Å from the O^+ $(2s^{-1}\,{}^4P^e)$ state was the only fluorescence wavelength which could be registered. The cross section for dissociative ionization from the ground state of molecular oxygen, O_2 $(X\,{}^3\Sigma_g^-)$, is presented in Fig. 10. The dissociative ionization cross section of O_2 does not show a threshold behavior, like the cross sections for photoionization of the ground state of atomic oxygen. The energetical threshold at 33.6 eV for the dissociative ionization of O_2 results from threshold energy for photoionization out of the atomic oxygen ground state to the O^+ $(2s^{-1}\,{}^4P^e)$ state (28.5 eV) plus a dissociation energy of at least 5.1 eV. In our experimental observations, the dissociative ionization cross section is seen to increase from around 35 eV to a maximum (0.18 Mb) at around 42 eV before falling off monotonically as the energy is increased.

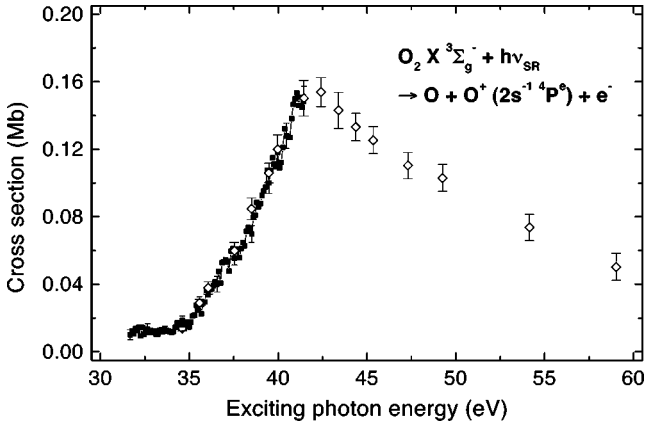

FIG. 10. Present experimental results for the dissociative ionization cross section for the process $O_2(X\,{}^3\Sigma_g^-)+h\nu_{SR}\rightarrow O+O^+(2s^{-1}\,{}^4P^e)+e^-$. The solid squares are taken from the 100-meV scanning experiment, and the open diamonds are from the measured spectra. Error bars include only statistical errors.

VI. CONCLUSIONS

Absolute cross sections for the $2s$-electron photoionization into the final ionic states O^+ $(2s^{-1}\,{}^4P^e, {}^2D^e, {}^2S^e, {}^2P^e)$ and for the occupation of the O^+ $(3s^{2,4}P^e)$ satellite states have been determined experimentally by PIFS. The measured cross sections agree within a factor of 2 with the theoretical predictions using the *ab initio R*-matrix approach. This is also the experimental uncertainty which is dominated by a systematic error in the normalization procedure. Meaningful conclusions can be drawn for cross section ratios which are in suitable harmony with experimental measurements for $2s^{-1}$ removal or $3s$-satellite excitation, but not for the cross-section ratio of $2s^{-1}$ removal to $3s$-satellite excitation.

Clearly higher photon energy resolution (10 meV or better) is desirable to delineate the autoionization states of atomic oxygen, together with greater photon flux, dissociation fragmention, and target state densities in these extremely difficult experiments. Further experimental work, perhaps performed at third generation light sources, would be desirable to test the absolute values of $2s^{-1}$ hole or $3s^{2,4}P^e$ satellite state theoretical photoionization cross sections with higher sensitivity.

ACKNOWLEDGMENTS

The experiments were financially supported by the Deutsche Forschungsgemeinschaft (DFG). The assistance of G. Reichardt at BESSY I and A. Werner in the preparation of

the experiments is gratefully acknowledged. The theoretical work was supported by grants from the German research council and by the AXAF Science Center (ASC) under a NASA grant to the Smithsonian Astrophysical Observatory at Harvard University. B.M.M. would like to thank Dr. Kate Kirby for many help discussions, and the hospitality and support of both the Institute for Theoretical Atomic and Molecular Physics (ITAMP) and the High Energy Astrophysics Division (HEAD) at the Harvard-Smithsonian Center for Astrophysics throughout the course of this research.

[1] G. G. Sirjee, Planet. Space Sci. **39**, 777 (1991).
[2] M. J. Seaton, in *Recent Studies in Atomic and Molecular Processes*, edited by A. E. Kingston (Plenum Press, New York, 1986), p.29.
[3] R. R. Meier (unpublished)
[4] R. R. Meier, Space Sci. Rev. **58**, 1 (1991).
[5] K. F. Dymond, S. E. Thonnard, R. P. McCoy, and R. J. Thomas, Radio Sci. **32**, 1985 (1997).
[6] D. J. Meléndez-Alvira, R. R. Meier, J. M. Picone, P. D. Feldman, and B. M. McLaughlin, J. Geophys. Res. **104**, 14 901 (1999).
[7] A. Dalgarno, M. B. McElroy, and R. J. Moffett, Planet. Space Sci. **11**, 463 (1963).
[8] A. Dalgarno and M. B. McElroy, Planet. Space Sci. **11**, 727 (1963).
[9] K. L. Bell, P. G. Burke, A. Hibbert, and A. E. Kingston, J. Phys. B **21**, 2319 (1989).
[10] K. L. Bell and R. P. Stafford, Planet. Space Sci. **40**, 1419 (1992).
[11] K. L. Bell and A. E. Kingston, Adv. At., Mol., Opt. Phys. **32**, 1 (1994).
[12] A. R. Striganov and N. S. Sventitskii, *Tables of Spectral Lines of Neutral and Ionized Atoms* (IFI/Plenum, New York, 1968).
[13] Based on H. Pauly, in *Atomic and Molecular Beam Methods*, edited by G. Scales (Oxford University Press, Oxford 1988), p. 83.
[14] O. Wilhelmi and K.-H. Schartner, Eur. Phys. J. D (to be published); *ibid.* (to be published).
[15] R. R. Laher and F. R. Gilmore, J. Phys. Chem. Ref. Data **19**, 277 (1990).
[16] S. J. Schaphorst, M. O. Krause, C. D. Caldwell, H. P. Saha, M. Pahler, and J. Jiménez-Mier, Phys. Rev. A **52**, 4656 (1995).
[17] J. A. R. Samson and V. E. Petrosky, Phys. Rev. A **9**, 2449 (1974).
[18] W. C. Stolte, Y. Lu, J. A. R. Samson, O. Hemmers, D. L. Hansen, S. B. Whitfield, H. Wang, P. Glans, and D. W. Lindle, J. Phys. B **30**, 4489 (1997).
[19] J. A. R. Samson and P. N. Pareek, Phys. Rev. A **31**, 1470 (1985).
[20] F. J. Comes, F. Speier, and A. Elzer, Z. Naturforsch. A **23A**, 125 (1968).
[21] P. B. Cairns and J. A. R. Samson, Phys. Rev. **139**, A1403 (1965).
[22] P. van der Meulen, C. A. de Lange, M. O. Krause, and D. C. Mancini, Phys. Scr. **41**, 837 (1990).
[23] O. Wilhelmi, G. Mentzel, B. Magel, K.-H. Schartner, A. Werner, S. Lauer, H. Schmoranzer, and F. Vollweiler, Phys. Lett. A **228**, 283 (1997).
[24] K. T. Taylor and P. G. Burke, J. Phys. B **9**, L353 (1976).
[25] K. L. Bell, K. A. Berrington, P. G. Burke, A. Hibbert, and A. E. Kingston, J. Phys. B **21**, 2319 (1990).
[26] G. C. Angel and J. A. R. Samson, Phys. Rev. A **38**, 5578 (1988).
[27] C. D. Caldwell and M. O. Krause, Phys. Rev. A **47**, R759 (1993).
[28] A. Menzel, S. Benzaid, M. O. Krause, C. D. Caldwell, U. Hergenhahn, and M. Bissen, Phys. Rev. A **54**, R991 (1996).
[29] B. M. McLaughlin and K. P. Kirby, J. Phys. B **31**, 4991 (1998).
[30] A. K. Pradhan, Planet. Space Sci. **28**, 165 (1980).
[31] A. F. Starace, S. T. Manson, and D. J. Kennedy, Phys. Rev. A **9**, 2453 (1974).
[32] R. J. W. Henry, Planet. Space Sci. **15**, 1747 (1967).
[33] J. L. Dehmer and P. M. Dehmer, J. Chem. Phys. **67**, 1782 (1977).
[34] H.-J. Flaig, K.-H. Schartner, E. Träbert, and P. H. Heckmann, Phys. Scr. **31**, 255 (1985).
[35] O. Wilhelmi, G. Mentzel, B. Zimmermann, K.-H. Schartner, H. Liebel, and H. Schmoranzer, J. Electron Spectrosc. Relat. Phenom. **101–103**, 155 (1999).
[36] J. A. Fennelly and D. G. Torr, At. Data Nucl. Data Tables **51**, 321 (1992).
[37] K. L. Bell, A. Hibbert, R. P. Stafford, and B. M. McLaughlin, Phys. Scr. **50**, 343 (1994).